Int. J. Electrochem. Sci., 16 **(2021)** Article Number: 211219, doi: 10.20964/2021.12.34

International Journal of
ELECTROCHEMICAL
SCIENCE
www.electrochemsci.org

Short Communication

The Inhibition Effect Mechanism of Pyrazole on Cobalt Corrosion in Alkaline Solution

Wenqian Zhang[1,*], *Tongju Wang*[1], *Suye Yu*[1], *Guorui Liu*[2,3,*], *Peng Zhao*[1], *Tiecheng Han*[1], *Liu Yang*[1]

[1] School of Electronic and Control Engineering, North China Institute of Aerospace Engineering, Langfang of Hebei Province 065000, China
[2] Computing Center, Tianjin Chengjian University, Tianjin 300380, China
[3] Institute of Microelectronics, Hebei University of Technology, Tianjin 300130, China
[*]E-mail: wqzhang226@163.com, lgr@tcu.edu.cn

Received: 5 August 2021 / *Accepted:* 15 September 2021 / *Published:* 10 November 2021

In order to protect cobalt from corrosion, finding an effective inhibitor is a focus of studies. In this paper, the inhibition effect and mechanism of pyrazole on cobalt corrosion was investigated by state etch rate (SER) test, potentiodynamic polarization measurement and DFT calculation. The results of SER and potentiodynamic polarization experiments both exhibited the similar corrosion and inhibition characteristics of pyrazole for cobalt: the corrosion of cobalt was inhibited at high concentration of pyrazole, but was accelerated at low concentrations in the citric-hydrogen peroxide system with a pH of 10.5. Meanwhile, the conclusion can also be drown that pyrazole is a mixed and relatively weak inhibitor for cobalt. Then the mechanism of pyrazole was further explored. Pyrazole exists mainly in molecular form in alkaline solution. The DFT calculation results indicate that on cobalt surface, the adsorption structure of vertical pyrazole molecule via nitrogen atom N2 site is the easiest and most stable. The inhibitory effect stems from the adsorption of the passivation film formed by hydrogen bonds between pyrazole molecules on the cobalt surface.

Keywords: pyrazole, inhibitor, cobalt, electrochemical, DFT calculation

1. INTRODUCTION

Diffusion barriers are commonly used to prevent the diffusion of copper into dielectric region in integrated circuit manufacturing[1]. Ta/TaN bilayer is widely used in Si-integrated circuit[1,2]. However, as the technology node reaches 14nm and below, to avoid problems such as inadequate gap-fill and pinched-off opening, cobalt (Co) replaces tantalum as liner material of barrier for copper interconnects due to its lower resistivity, higher thermal stability than tantalum and good step coverage

for copper[3-5]. The cobalt is prone to corrosion and the introduce of cobalt liner has brought new problems in the chemical mechanical polishing (CMP) process, including the corrosion inhibition of cobalt, the reduction of galvanic corrosion between copper and cobalt, and the removal rate selectivity control and so on. Actually, corrosion inhibitor of polishing slurry plays an important role in solving the above problems. Each component of the polishing liquid has different functions: abrasive is used for mechanical grinding, complexing agent and oxidant are used to accelerate the chemical reaction rate synergistically, surfactant is used to reduce the surface roughness of polished material and improve the stability and dispersion of slurry, and inhibitors are used to protect metal from chemical dissolution and reduce the galvanic corrosion, so that the removal rate selectivity and planarization performance can be improved. Finding an effective inhibitor to mitigate Co corrosion is a focus of Co CMP studies[6]. Inhibitors for cobalt have been extensively investigated by researchers. Sagi et al. [7] studied CMP of chemical vapor deposited Co films with minimal corrosion in the Cu/Co/Mn/SiCOH patterned structures. It is reported that nicotinic acid (NA) is effective in decreasing the dissolution and corrosion currents of cobalt by film loss measurement and electrochemical experiments. Yang et al. [8] reported that the galvanic corrosion of Cu/Co and pitting corrosion on cobalt surface were both reduced under the combination of benzotriazole (BTA) and 1-phenyl-3-methyl-5-pyrazolone (PMP). And the mechanisms of synergistic effect were proposed. He et al. [6] studied the 1,2,4-triazole (TAZ) as corrosion inhibitor for chemical mechanical polishing of cobalt in H_2O_2 based acid slurry. It is reported that TAZ can effectively inhibit the chemical corrosion for cobalt and galvanic corrosion between copper and cobalt under physical and chemical adsorption. But when the concentration of TAZ exceeds 100mM, the Co-TAZ complexes formed become unstable and cause pitting corrosion. Zhong et al. [9] also indicated TAZ is a good passivating agent for cobalt during post-CMP cleaning. Hu et al. [10] and Zhang et al. [11] investigated the effect of 2,2'-{[(methyl-1H-benzotriazol-1-yl)methyl]imino}bisethanol (TT-LYK) as corrosion inhibitor on cobalt chemical mechanical polishing from experimental and density functional theory. The results show that in H_2O_2-based slurry, TT-LYK both has good inhibitory effect on cobalt whether potassium tartrate or nitrilotriacetic acid as complexing agent. Meanwhile, TT-LYK is proved that it is helpful to reduce the galvanic corrosion between copper and cobalt. Lu et al. [12] studied the effect of H_2O_2 and 2-Mercaptothiazoline (2-MT) on the CMP of cobalt adhesion layer in acid slurry. It is reported that 2-MT can greatly prevent cobalt from corrosion and is efficient to reduce the static etch rate and removal rate of cobalt in glycine based slurry. Various inhibitors have been studied, however, there is still a dearth of research on pyrazole as inhibitor for cobalt.

Pyrazole, also known as 1,2-diazole, is soluble in water, alcohol, ether and benzene. And it has a wide range of applications in organic synthesis. Geler et al. [13] and Yang et al. [14] respectively reported that pyrazole has a good corrosion inhibition effect on copper no matter in acidic or alkaline medium. Goswami et al. [15] also demonstrated that pyrazole is an effective copper corrosion inhibitor in a pH 14 TMAH as a model post CMP cleaning solution. However, the effect of pyrazole on cobalt needs to be further explored. In this work, the inhibition effect and mechanism of pyrazole on cobalt corrosion were investigated by extensive experimental investigations and density functional theory (DFT) analysis. Static etch rates and potentiodynamic polarization plots were tested and then the inhibition mechanism was discussed by functional theory.

2. EXPERIMENTAL

2.1. Solutions preparation.

The solutions used were prepared with deionized (DI) water and analytical reagent grade chemicals. Citric acid and hydrogen peroxide (H_2O_2) were used as complexing agent and oxidizer, respectively. Pyrazole (abbreviated as Pz, $C_3H_4N_2$) was employed as corrosion inhibitor for cobalt, whose chemical structure is presented in Fig.1. The solutions consists of 10mM citric acid and 5ml/L H_2O_2 and pyrazole with different concentrations. The pH was adjusted to 10.5 using diluted KOH and HNO_3. No abrasives were added to the solutions to eliminate other disruptive factors such as adsorption on the cobalt electrode.

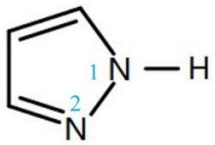

Figure 1. The chemical structure of pyrazole.

2.2. Static etch rate experiments.

The static etch rates (SER) of cobalt were tested in room temperature by using a 99.99% pure cobalt disk (Φ=3 inch，1 inch = 2.54 cm). Prior to SER test, cobalt disk was polished by metallographic pre-grinding machine and then by 2000 grit sandpaper, rinsed in DI water and dried. The cobalt disk were immersed for 9 mins in solutions with different concentration of pyrazole respectively. The SER of cobalt was obtained by measuring the weight loss using a FA2204C analytical balance (Techcomp, Inc.). Each test was performed three times and averaged.

2.3. Electrochemical experiments.

Electrochemical experiments were performed using a CorrTest CS310H electrochemical workstation (CorrTest company, Wuhan, China). A Pt sheet (20×20×0.2 mm) was used as the counter electrode, a Hg/HgO electrode was utilized as the reference electrode and a cobalt coupon (10×20×2 mm) sealed with epoxy resin to expose a $1cm^2$ working aera was employed as the working electrode, respectively. The potentiodynamic polarization plot was measured after 600s open circuit potential (OCP) test. The voltage range was set as E_{oc}±0.3 V and the scan rate was set as 5 mV/s.

2.4. Computational details.

Spin polarized DFT calculations were carried out using the Vienna ab initio simulation package (VASP) code[16,17]. All calculations were done with the generalized gradient approximation (GGA)

approach of Perdew, Burke and Ernzerhof (PBE) [18-19]. The plane wave cutoff energy was set to 400eV. The k-point mesh was generated by automatic Monkhorst-Pack scheme[20]. After examination, 4×4×1 k-point mesh was accurate with its changes in energies smaller than 2 meV/atom. Besides, cobalt exists in the hexagonal close-packed (hcp) structure below 700 K, and the (0001) direction of hcp structure is the only crystal direction with relative high symmetry operations [21,22]. So the hcp Co(0001) surface was employed to calculate. The simulation cells contained a slab formed four-layer cobalt atoms (a total of 64 cobalt atoms) and on which a vacuum space of 30 Å in the Z direction. All atoms in the top two layers of the slab were relaxed while the bottom two-layers were fixed at the corresponding bulk positions [23].

The reference total energy calculations of pyrazole molecule was carried out using a cubic box with size of 15×15×15 $Å^3$ with gamma point for the k-point sampling [23]. Finally, the pyrazole molecule was positioned 3~4 Å on the cobalt surface along the Z direction to simulate the adsorption process.

3. RESULTS AND DISCUSSION

3.1. State etch rate measurement

The solution composed of 10mM citric acid and 5ml/L H_2O_2 at pH 10.5 was used as the reference solution, denoted as Ref. Fig.2 shows the SER of cobalt in the reference solution containing different pyrazole concentration. The results show that the SER first increases and then decreases as the concentration of pyrazole increases. When the concentration is 10mM and 50mM, the SER is higher than that without pyrazole. In the absence of pyrazole, the corrosion of cobalt is severe mainly due to the synergistic effect of citric acid and hydrogen peroxide. $Co(OH)_2$ is formed on cobalt surface, and ionized Co^{2+} ($Co(OH)_2$ f $Co^{2+}+2OH^-$) complexes with the deprotonated Citrate ion L^{3-} (L refers to $C_6H_5O_7$) to form a soluble complex ($Co^{2+}+2L_3^- \rightarrow (CoL_2)^{4-}$)[24,25]. At low concentration of pyrazole，localized dissolution is accelerated due to the uneven coverage of pyrazole on cobalt surface, resulting in corrosion promotion like a complexing agent. As the concentration of pyrazole continues to increased, a adsorption passivation film is formed and the surface reaction is suppressed due to the accumulation and adsorption of pyrazole on the cobalt surface, thereby the SER of cobalt was gradually reduced. Similar phenomenon also occurs in other inhibitors such as benzotriazole (BTA) and 1,2,4-triazole for cobalt[26,27]. In summary, pyrazole exhibits corrosion inhibitory effects on cobalt, however, it also can be seen from the results that pyrazole is a relatively weak inhibitor for cobalt because of the relatively high concentration used.

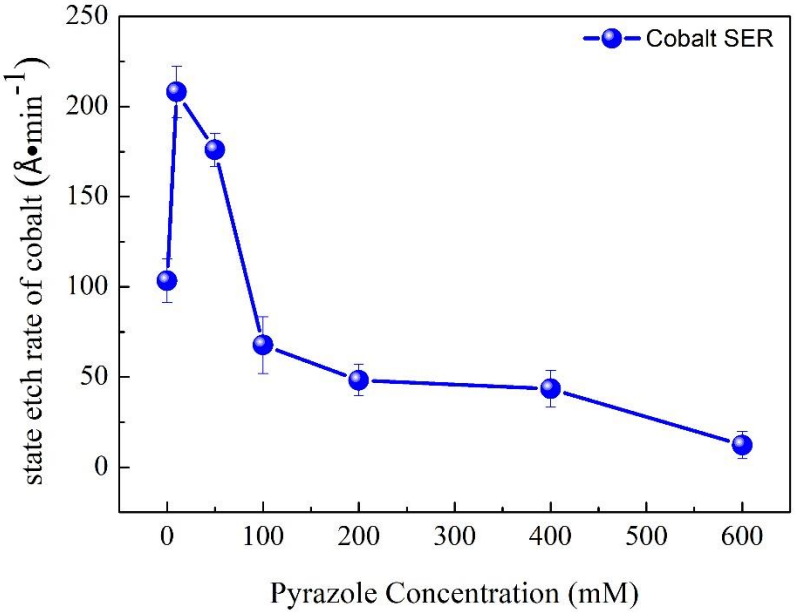

Figure 2. SER of cobalt in reference solution containing different concentration of pyrazole at pH 10.5.

3.2. Potentiodynamic polarization analysis

The effect of pyrazole on cobalt was further studied by electrochemistry. Fig.3 shows the potentiodynamic polarization curves of cobalt in reference solutions containing different concentration of pyrazole. The detailed parameters including corrosion current density i_{corr}, corrosion potential E_{corr}, the anodic and cathodic Tafel slops (β_a and β_c) were calculated with the CS Studio5 software by linear fitting in the anodic and cathodic Tafel regions, which is shown in Table 1. According to the results, all the curves of cobalt exhibit the similar polarization behaviors. As the pyrazole concentration increases from 0 mM to 400 mM, the polarization curve first shifts to the right and then to the left, and the I_{corr} firstly reaches to 28.424 μA/cm^2 from 18.929 μA/cm^2 and then declines to 9.2873 μA/cm^2, implying that the corrosion of cobalt was promoted at the pyrazole concentration less than 100mM and was inhibited when the concentration of pyrazole exceeded 100mM. At low concentration such as 10mM and 50mM, pyrazole adsorbs at individual sites of cobalt, however, a small amount of pyrazole is difficult to form dense passivation film on cobalt surface. On the contrary, the cobalt surface becomes active, making the electronic transfer on electrode accelerated and corrosion current of cobalt increased. At high concentration, a dense adsorption film composed of pyrazole covers the cobalt surface, resulting in the electrode reaction prevention and corrosion current reduction. The cathodic and anodic Tafel slopes (β_a and β_c) are in direct proportion to the resistance of electrode reaction [28,29]. The slight upward trend of β_a and β_c indicates that the electron transfer becomes more difficult in the electrode reaction, namely, the passive film on cobalt has a better dissolution resistance. Moreover, there is almost no obvious change in corrosion potential（change range of E_{corr} within 24 mV），indicating that pyrazole is a mixed inhibitor for cobalt. Inhibition efficiency (IE) given in Table 1 was calculated according to Equation 1. The inhibition efficiency is only 50.96% at the pyrazole concentration of 400mM. However,

when the concentration is increased to 600mM, the inhibition efficiency decreases to 49.41%, which also indicates that pyrazole is a relatively weak inhibitor for cobalt. This is consistent with the observation from SER results.

$$IE = \frac{i_{corr,0} - i_{corr}}{i_{corr,0}} \times 100 \quad (1)$$

where $i_{corr,0}$ and i_{corr} are the current density of cobalt in the absence and presence of pyrazole, respectively.

Table 1. Fitted values of parameters from potentiodynamic polarization curves described in Fig.3.

Concentration (mM)	icorr（μA/cm^2）	βa（mV）	βc（mV）	Ecorr（V）	IE (%)
0	18.929	56	55	-0.198	—
10	28.424	55	54	-0.212	—
50	19.817	57	55	-0.204	—
100	17.2	58	57	-0.188	9.13
200	10.968	59	63	-0.208	42.01
400	9.2837	61	65	-0.203	50.96
600	9.5763	62	62	-0.210	49.41

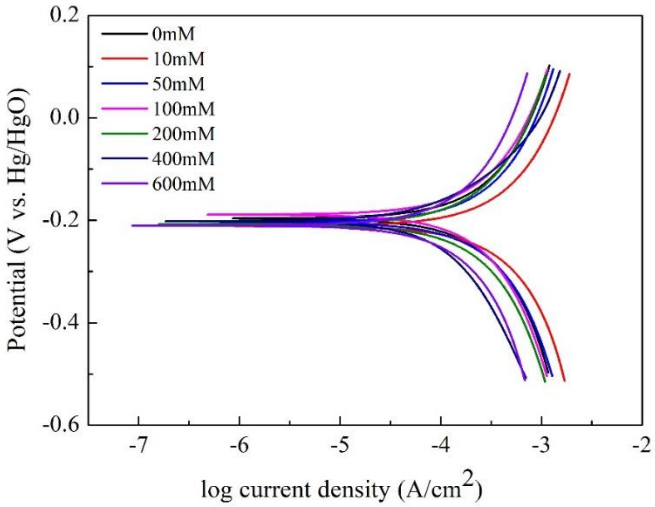

Figure 3. Potentiodynamic polarization curves of cobalt in reference solutions containing different concentration of pyrazole at pH 10.5.

3.3. Mechanism of pyrazole on cobalt.

3.3.1. Species and distribution of pyrazole

In order to investigate the mechanism of pyrazole on cobalt surface, it is necessary to know the species of pyrazole that plays the corrosion inhibitor under alkaline condition. As shown in the structure

of Fig.4, there are three species of pyrazole including protonated pyrazole, pyrazole and deprotonated pyrazole, which are abbreviated as Pz^+, Pz and Pz^-, respectively. The distribution of pyrazole species is determined by the pH of solution. According to the dissociation constant of pyrazole (pKa1=2.52[30,31], pKa2=14.21[31]), the distribution of pyrazole species at various pH values presented in Fig.4 can be calculated by the Henderson-Hasselbalch equation [32]. It is obvious that Pz species accounts for 99.98% at pH 10.5, therefore, it can be conclude that the inhibitory effect of pyrazole is mainly due to the adsorption of pyrazole molecules on cobalt surface rather than the reaction of Pz^- and Co^{2+}. Pyrazole is an N-heterocyclic aromatic compound comprised of carbon, nitrogen and hydrogen, where carbon and hydrogen are non-polar groups and nitrogen is polar groups. In general, polar groups have stronger electronegativity than non-polar groups, so the nitrogen is more negatively charged and easier to bridge with cobalt than carbon and hydrogen. It can be preliminarily concluded that pyrazole molecules are adsorbed on cobalt surface mainly through N1 or N2 positions. The specific adsorption position needs to be further studied.

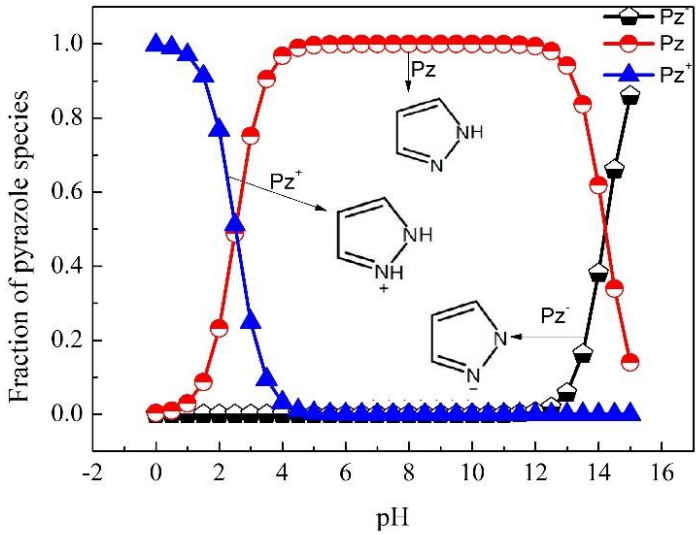

Figure 4. Species and distribution of pyrazole at various pH values.

3.3.2. Adsorption structure of pyrazole molecule on Co(0001)

DFT calculation was employed to investigate the structure model of pyrazole molecule on Co(0001) surface. The structure of pyrazole and cobalt slab was firstly optimized and then three initial adsorption models were built to simulate. Fig.5 shows the parallel and vertical adsorption structures of pyrazole molecule on Co(0001) surface with no interactions. Fig.5 (a) shows that the pyrazole molecule was parallel positioned at a distance of 4 Å from the first layer atoms of Co(0001). Fig.5 (b) and (c) respectively shows that the nitrogen atom N1 position and N2 position of pyrazole molecule was vertically placed 4 Å away from the first layer of cobalt atoms. The optimized structures between pyrazole molecule and Co(0001) surface are presented in Fig.6. As observed in Fig.6 (a), the parallel placed pyrazole molecule was tilted and tend to adsorb on cobalt surface via N2 site. Meanwhile, the distance between Co atoms and nitrogen atom N2 was decreased to 2.042 Å. The N1 position (N-H

bond) didn't interact with Co(0001) in Fig.6 (b) while the N2 position directly binds to Co(0001) in Fig.6 (c) (the distance of Co-N2 is 2.036 Å). The above results indicate that the adsorption position is N2 site. The adsorption energy (E_{ads}) was further calculated by Equation 2 and the results are listed in Table 2.

$$E_{ads} = E_{Co-pyrazole} - E_{pyrazole} - E_{Co} \quad (2)$$

where $E_{Co\text{-}pyrazole}$ is the total energy of Co(0001) surface with adsorbed pyrazole molecule, $E_{pyrazole}$ is the energy of pyrazole molecule and E_{Co} is the energy of cobalt slab. The adsorption energy E_{ads} corresponding to the three structures in Fig.6 are -0.862eV, -0.413eV and -0.880eV, respectively. The adsorption energy is all negative, indicating that the adsorption of pyrazole molecule on cobalt surface is spontaneous and exothermic[33].The more negative E_{ads} is, the stronger adsorption is[34]. That is, the model of vertical pyrazole molecule via N2 site adsorbed on the Co(0001) surface is easier and more stable than the other two models.

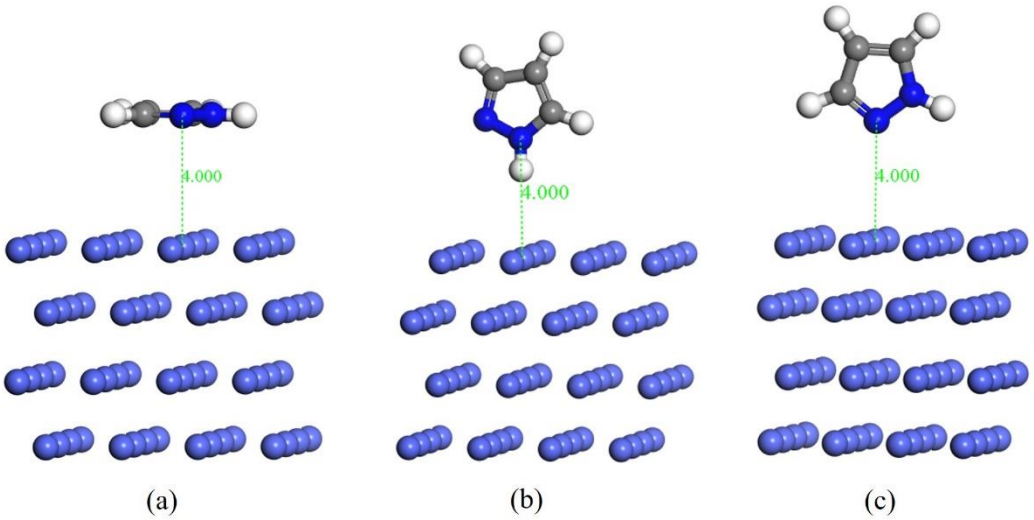

Figure 5. Initial adsorption structures of (a) parallel pyrazole molecule; (b) vertical pyrazole via nitrogen atom N1; (c) vertical pyrazole via nitrogen atom N2 on Co(0001) surface with no interactions.

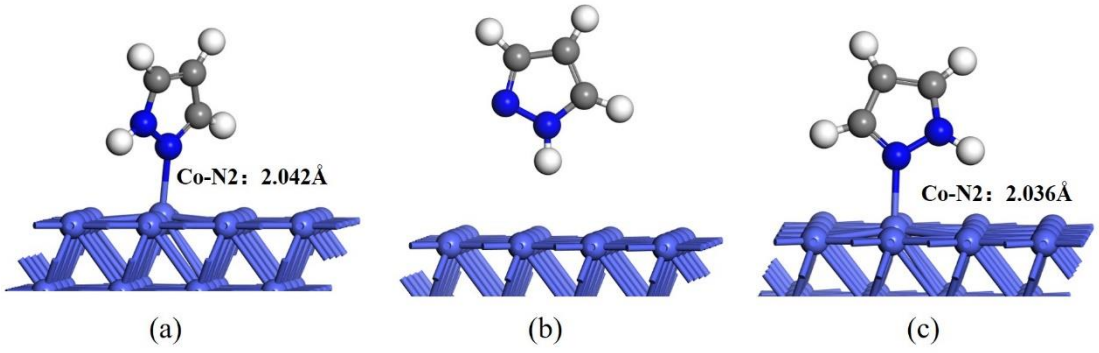

Figure 6. Optimized structures of (a) parallel pyrazole; (b) vertical pyrazole via nitrogen atom N1; (c) vertical pyrazole nitrogen atom N2 on Co (0001) surface.

On the basis of above research, the adsorption mechanism of pyrazole molecule on cobalt surface is proposed. Pyrazole mainly exists in molecule form in solution with pH of 10.5, and vertical pyrazole molecule interacts with cobalt atom via nitrogen atom N2 site. Then an adsorption film on cobalt surface can be formed, which is composed of pyrazole molecules connected by intermolecular hydrogen bonds. When the concentration of pyrazole is sufficient for the adsorption film to evenly cover the cobalt surface, the inhibitory effect of pyrazole works to protect cobalt from corrosion.

Table 2. The adsorption energy for different models.

Models	$E_{Co\text{-}pyrazole\ (eV)}$	$E_{ads\ (eV)}$
parallel	-467.102	-0.862
N1, vertical	-466.653	-0.413
N2, vertical	-467.120	-0.880

$E_{pyrazole=-57.510eV;}$ $E_{Co=\ -408.730eV}$

4. CONCLUSIONS

The effect and mechanism of pyrazole on cobalt was investigated in alkaline medium from experimental and theoretical calculations. The conclusions are as follows:

(1) The corrosion and passive properties of pyrazole on cobalt is related to the concentration. SER and potentiodynamic polarization experiments exhibited the similar phenomenon. When the pyrazole concentration was lower than 100mM, corrosion of cobalt was promoted. Above 100 mM, the inhibition of pyrazole on cobalt began to appear. But when the concentration was 400 mM, the inhibition efficiency is only 50.96%.

(2) The main species of pyrazole is molecule at pH 10.5, which accounts for 99.98%.

(3) DFT calculation results show that the adsorption energy of vertical pyrazole molecule via N2 site is more negative (-0.880eV), implying this structure is more stable than vertical structure via N1 site and parallel structure on Co(0001) surface. Therefore, the inhibitory property of pyrazole is attributed to the adsorption film formed by connecting pyrazole molecules via N2 site on cobalt surface.

However, pyrazole is a relatively weak inhibitor for cobalt. In order to reduce the use concentration and improve the inhibition efficiency, it is necessary to find some other inhibitors used in combination with pyrazole. Meanwhile, the synergy mechanism needs to be further studied in the future.

ACKNOWLEDGMENTS
This work was financially supported by the Education Department Science Research project of Hebei under Grant No.QN2020102, the Doctoral Research Fund of North China Institute of Aerospace Engineering under Grant No.BKY201803 and BYK202116, and the Major Project of the Science and Technology Ministry in Hebei Province under Grant No.21280201Z. I also would like to thank many group members for assisting with data collection, data analysis, data interpretation and helpful discussions.

References

1. B.S. An, Y. Kwon, J.S. Oh, C. Lee, S. Choi, H. Kim, M. Lee, S. Pae and C.W. Yang, *ACS Appl. Mater. Interfaces*, 12 (2020) 3104.
2. Q. Xie, X.P. Qu, J.J Tan, Y.L. Jiang, M. Zhou, T. Chen and G.P. Ru, *Appl. Surf. Sci.*, 253 (2006) 1666.
3. Y. Kadam, U. Yerramilli, and A. Bahadur, *Colloids Surf B Bioibterfaces*, 72 (2009) 141.
4. L. Jiang, Y. Y. He, Y. Li, Y. Z. Li, and J. B. Luo, *Microelectron. Eng.*, 122 (2014) 82.
5. B. C. Peethala, H. P. Amanapu, U. R. K. Lagudu and S. V. Babu, *J. Electrochem. Soc.*, 159 (2012) 582.
6. P. He, B.B. Wu, S. Shao, T. Teng, P. Wang and X.P. Qu, *ECS J. Solid State Sci. Technol.*, 8 (2019) 3075.
7. K. V. Sagi, L. G. Teugels, M. H. V. D. Veen, H. Struyf, S. R. Alety and S. V. Babu, *ECS J. Solid State Sci. Technol.*, 6 (2017) 276.
8. S.H. Yang, B.G. Zhang, Q.M. Zhang, R. Wang, X. Yu, C.W. Wang and Y.L. Liu, *ECS J. Solid State Sci. Technol.*, 8 (2019) 416.
9. M. J. Zhong, S. S. Venkataraman, Y. Q. Lan, Y. Z. Li and Devon A. Shipp, *ECS J. Solid State Sci. Technol.*, 161 (2014) 138.
10. L.J. Hu, G.F. Pan, H. Wang, X.B. Zhang, Z.Y. Wang and T.T. Zhu, *Mater. Chem. Phys.*, 256 (2020) 12367.
11. X.B Zhang, G.F. Pan, L.J. Hu, H. Wang and C.W. Wang, *Colloids Surf. A*, 605 (2020) 125392.
12. H.S. Lu, J.X. Wang, X. Zeng, F. Chen, X.M. Zhang, W.J. Zhang and X.P. Qu, *Electrochem. Solid-State Lett.*, 15 (2012) 97.
13. E. Geler, D.S. Azambuja, *Corros. Sci.*, 42 (2000) 631.
14. W.Z. Yang, Y.H. Wang, Y.M. Tang and B. Yu. *Corros. Sci. Prot. Technol.*, 17 (2005) 314.
15. A. Goswami, S. Koskey, T. Mukherjee and O. Chyan, *ECS J. Solid State Sci. Technol.*, 3 (2014) 293.
16. F.F. Ma, S.H. Ma, Z.Y. Jiao and X.Q. Dai, *Appl. Surf. Sci.*, 384 (2016) 10.
17. Y.B. Xue, Y.T. Zhou, D. Chen and X.L. Ma, *J. Alloy. Comp.*, 582 (2014) 181.
18. C. William, R. Antonio, M. O. Jose` and J. M. Feliu, *J. Phys. Chem. C*, (DOI:10.1021/acs.jpcc.8b03852)
19. J. P. Perdew, K. Burke and M. Ernzerhof, *Phys. Rev. Lett.*, 77 (1996) 3865.
20. 20. L.B. Gisela, A. J. Adamczyk, *Surf. Sci.*, 688(2019) 31.
21. R. Lizárraga, F. Pan, L. Bergqvist L, E. Holmstrom, Z. Gercsi and L. Vitos, *Scientific Reports*, 7 (2017) 3778.
22. C. Li, A.J. Freeman and C.L. Fu, *J. Magn. Magn. Mater.*, 94 (1991) 134.
23. S.Y. Yu, X. Ju, C.B. Wan and S.N. Li, *Int. J. Hydrogen Energ.*, 40 (2015) 6365.
24. A. M. N. Silva, X.L. Kong and R. C. Hider, *Biometals*, 22 (2009) 771.
25. C. Ling, F.Q. Liu, Z.G. Pei, X.P. Zhang, M.M. Wei, Y.H. Zhang, L.R. Zheng, J. Zhang, A.M. Li and B.S. Xing, *Scientific Reports*, 5 (2015) 09944.
26. W.Q. Zhang, Y.L. Liu, C.W. Wang, X.H. Niu, J. Ji, Y.C. Du and L.N. Han, *ECS J. Solid State Sci. Technol.*, 6 (2017) P786.
27. H. S. Lu, Investigation of Chemical Mechanical Polishing of Novel Diffusion Barrier Co/TaN for Cu interconnect, Fudan University, Shanghai, China, 2013, 121.
28. W.M. Tian, S.M. Li, B. Wang, J.H. Wang and M. Yu, *Corros. Sci.*, 113 (2016) 1.
29. W.M. Tian, Z.L. Li, H.F. Kang, F.S. Cheng, F.F. Chen and G.X. Pang, *Materials*, 13 (2020) 3236.
30. A. N. Kost and I. I. Grandberg, *Adv. Heterocycl. Chem.*, (1966) 347.
31. J. Alvarez-Builla, J. J. Vaquero and J. Ba Rluenga, Modern heterocyclic chemistry Vol.1. *Wiley-VCH Verlag & Co*, (2011) 1047. (DOI: 10.1002/9783527637737)
32. L. J. Henderson, *American Journal of Physiology-Legacy Content*, 21(1908) 427. (DOI:

141.002.140.067)
33. D. Masego, O. O. Lukman, E. F. Omolola, Y. Sasikumar, R. Baskar, B. Indra, S. A. Abolanle, M. K. Mwadham and E. E. Eno, *Molecules*, 20 (2015) 15701.
34. B. Yang, K. Shi, H. Li, L. Jiang and C.H. Zhang, *Indian J. Phys.*, 93 (2019) 1019.